Article

Photosynthesis re-wired on the pico-second timescale

https://doi.org/10.1038/s41586-023-05763-9

Received: 31 January 2022

Accepted: 26 January 2023

Published online: 22 March 2023

Check for updates

Tomi K. Baikie[1,7], Laura T. Wey[2,3,7], Joshua M. Lawrence[2,4], Hitesh Medipally[5], Erwin Reisner[4], Marc M. Nowaczyk[5,6], Richard H. Friend[1], Christopher J. Howe[2]✉, Christoph Schnedermann[1]✉, Akshay Rao[1]✉ & Jenny Z. Zhang[4]✉

Photosystems II and I (PSII, PSI) are the reaction centre-containing complexes driving the light reactions of photosynthesis; PSII performs light-driven water oxidation and PSI further photo-energizes harvested electrons. The impressive efficiencies of the photosystems have motivated extensive biological, artificial and biohybrid approaches to 're-wire' photosynthesis for higher biomass-conversion efficiencies and new reaction pathways, such as H_2 evolution or CO_2 fixation[1,2]. Previous approaches focused on charge extraction at terminal electron acceptors of the photosystems[3]. Electron extraction at earlier steps, perhaps immediately from photoexcited reaction centres, would enable greater thermodynamic gains; however, this was believed impossible with reaction centres buried at least 4 nm within the photosystems[4,5]. Here, we demonstrate, using in vivo ultrafast transient absorption (TA) spectroscopy, extraction of electrons directly from photoexcited PSI and PSII at early points (several picoseconds post-photo-excitation) with live cyanobacterial cells or isolated photosystems, and exogenous electron mediators such as 2,6-dichloro-1,4-benzoquinone (DCBQ) and methyl viologen. We postulate that these mediators oxidize peripheral chlorophyll pigments participating in highly delocalized charge-transfer states after initial photo-excitation. Our results challenge previous models that the photoexcited reaction centres are insulated within the photosystem protein scaffold, opening new avenues to study and re-wire photosynthesis for biotechnologies and semi-artificial photosynthesis.

The photodynamics of Photosystems I and II have been extensively studied in vitro using ultrafast TA spectroscopy[6]. In this technique, the sample's absorbance spectrum is measured by a broadband probe laser after photo-excitation by a pump laser (that is, pump-probe spectroscopy), with access to photodynamics occurring on the subpico-second timescale. Previously, it has been challenging to apply ultrafast TA spectroscopy on the photosystems in vivo, with plant or algal cells (typically 10 µm in size)[7] being highly scattering. Recently, ultrafast TA spectroscopy was successfully applied to *Nannochloropsis* sp. algal cells (2–5 µm in size)[8], whose small size lessened these scattering effects[9]. Here, we studied *Synechocystis* sp. PCC 6803 (hereafter *Synechocystis*) cyanobacterial cells (Fig. 1a–c), which is a model organism for studying photosynthesis because of the endosymbiotic origin of the chloroplast in eukaryotic plants and algae[10]. The smaller size of *Synechocystis* cells (less than 2 µm)[11] further reduced the scattering, and the photodynamics of the photosystems in vivo could be resolved using ultrafast TA spectroscopy.

Photo-excitation of *Synechocystis* cells with a 200 fs pump pulse centred at 450 nm revealed rich initial transient spectral features in the visible (550–800 nm). We identified a prominent negative feature at 685 nm (Fig. 1d), which decayed within roughly 20 ps to 10% of its initial value. We attribute this feature to the ground-state bleaching of the photoactive reaction centres of PSI and PSII. A lower-energy feature at 715 nm grew within roughly 2 ps after photo-excitation and subsequently decayed on a longer pico-second timescale, indicating rapid excited state relaxation processes. Similarly, we observed higher-energy positive transient features (less than 680 nm), which we assign to contributions from the photo-induced absorption of phycobilisomes (PBSs) and carotenoids, as these features resemble those of in vitro steady state absorption measurements[12,13] and are absent from isolated photosystems (Supplementary Fig. 7). We verified that the photosystems remained intact without photodamage, consistent over several biological replicates, and were in a closed state throughout these measurements (Supplementary Figs. 1–4). We confirmed that the key spectral features arise from fully assembled photosystems (Supplementary Information section 1.5.4.).

To probe the effect of exogenous electron mediators on the photodynamics of cyanobacterial cells, we repeated the same measurements with the addition of DCBQ. As shown in Fig. 1e, we found that addition of DCBQ led to accelerated decay dynamics of the negative feature at 685 nm. Simultaneously, the signal rise observed at 715 nm was suppressed, with a noticeable effect evident in just 600 fs after photo-excitation. The effect was also observed when pumping at the

[1]Cavendish Laboratory, University of Cambridge, Cambridge, UK. [2]Department of Biochemistry, University of Cambridge, Cambridge, UK. [3]Department of Life Technologies, University of Turku, Turku, Finland. [4]Yusuf Hamied Department of Chemistry, University of Cambridge, Cambridge, UK. [5]Plant Biochemistry, Ruhr University Bochum, Bochum, Germany. [6]Department of Biochemistry, University of Rostock, Rostock, Germany. [7]These authors contributed equally: Tomi K. Baikie, Laura T. Wey. ✉e-mail: ch26@cam.ac.uk; cs2002@cam.ac.uk; ar525@cam.ac.uk; jz366@cam.ac.uk

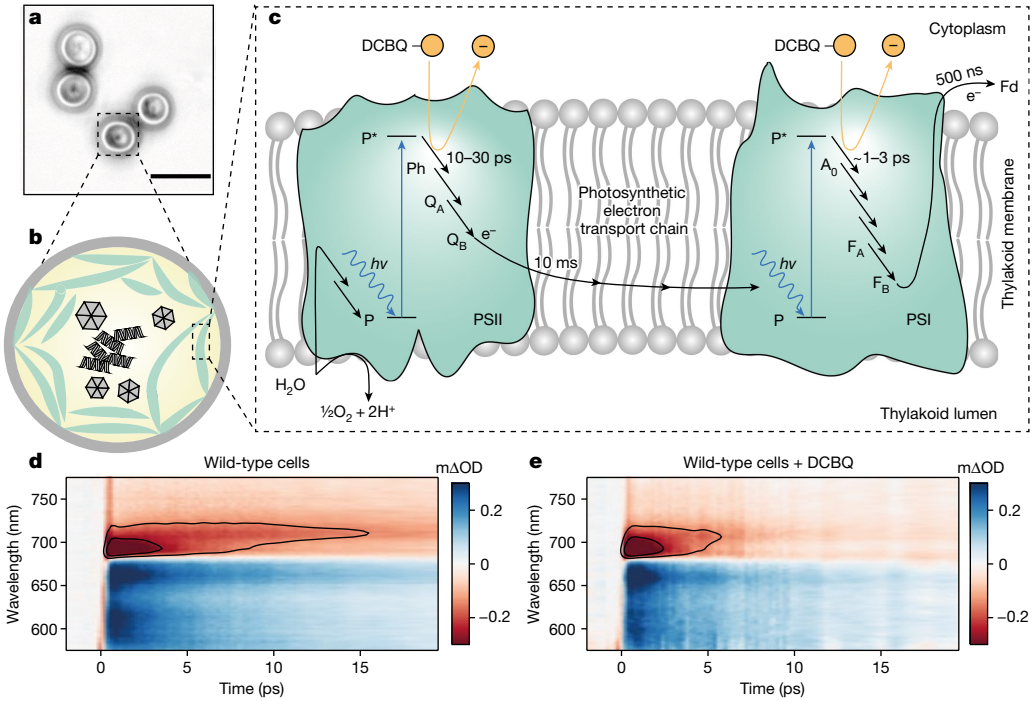

Fig. 1 | Exogenous electron mediator acts on the pico-second timescale in living cells. a, Bright field microscopy of *Synechocystis* sp. PCC 6803 cells. Scale bar, 5 µm. **b**, Schematic of a cell showing intracellular thylakoid membranes (green). **c**, Schematic of a simplified photosynthetic electron transport chain. The chain starts with PSII, in which a special pair of chlorophylls known as P680 is photoexcited to P680* directly or by energy transfer from other chlorophylls. An initial charge separated state with the primary electron acceptor pheophytin (Ph) [$P680^+$–Ph^-] is formed with a lifetime of 10–30 ps (ref. [34]) driving water oxidation. The extracted electrons exit PSII through terminal plastoquinones Q_A and Q_B. The electrons are shuttled along the chain, with the first diffusion step at roughly 10 ms (ref. [35]). The electrons are received by PSI and with further input of light, the P700 is photoexcited to P700* and an initial charge separated state with the primary electron acceptor chlorophyll A_0 [$P700^+$–A_0^-] is formed with a lifetime of roughly 1–3 ps (ref. [36]). The electrons exit PSI through the terminal iron-sulfur clusters F_A and F_B. The electrons are shuttled through ferredoxin (Fd) that takes around 500 ns (ref. [37]) and then onto various pathways, including the Calvin–Benson cycle. On the addition of the electron mediator DCBQ (orange circle), a new electron transfer pathway forms (orange arrow). **d**,**e**, Ultrafast TA spectroscopy map of wild-type cells (**d**) and cells with DCBQ (**e**) (5 mM) between −2 and 20 ps photo-excited at 450 nm in units of differential absorption (mΔOD). Two contours have been drawn at the same signal intensity to highlight the reduced lifetime of the 685 nm feature and suppression of the 715 nm rise on the addition of DCBQ. Maps are one sample, representative of several biological replicates (cells, $n = 8$, + DCBQ, $n = 5$).

band edge of the reaction centres (Supplementary Figs. 5 and 6). These observations demonstrate that DCBQ can alter the excited state decay pathways of the photosynthetic reaction centres in *Synechocystis* cells on a subpico-second timescale.

Previously, DCBQ has been thought to extract electrons only from the terminal electron acceptor site of PSII, the Q_B pocket (Fig. 1c). However, we note that the mid-point potential of DCBQ (+0.315 V versus standard hydrogen electrode (SHE) at pH 7)[14] makes it suitable for extracting electrons from both PSI ($P700^*/P700^+ = -1.290$ V, $F_B/F_B^- = -0.590$ V)[15] and PSII ($P680^*/P680^+ = -0.660$ V)[16]. To rule out energy transfer from the reaction centres to DCBQ as the mechanism resulting in the observations shown in Fig. 1e, we characterized the optical properties of suspensions of cells in the presence of DCBQ. As reported in Fig. 2b, the absorption spectrum of cells includes prominent absorption bands at 450, 680 and 700 nm corresponding primarily to the chlorophylls in the cell's PSII and PSI complexes, whereas DCBQ absorbs below 300 nm. The lack of overlap in the absorption spectra of DCBQ before reduction and fluorescence of the intact cells indicates that energy transfer mechanisms in the form of Förster resonances are not active[9]. After considering possible quenching mechanisms, we conclude that the effect caused by DCBQ must stem from an electron transfer mechanism (more detail in Supplementary Information section 1.5.5.).

It is known that all chlorophylls embedded within PSII and PSI are energetically degenerate at room temperature. Photo-excitation thus results in a highly delocalized excited state shared across several chlorophylls[17,18]. Previous studies on isolated reaction centres from the photosynthetic purple non-sulfur bacterium *Rhodobacter sphaeroides* at 77 K showed that the initially excited state shows charge-transfer character and can form intermediate charge-transfer states within 200 fs (ref. [19]). Similarly, recent femtosecond crystallography results of the photosynthetic reaction centre of another purple non-sulfur bacterium *Blastochloris viridis* (formerly known as *Rhodopseudomonas viridis*) demonstrated electron transfer reactivity within 3 ps (ref. [20]).

In the light of these observations, we postulate that photo-excitation of the chlorophyll pigments within the photosystems of *Synechocystis* at room temperature can also form highly delocalized intermediate charge-transfer states within the time resolution of our measurement (200 fs), followed by electron transfer kinetics. Given that the cell absorption spectra for all DCBQ concentrations remained unchanged (Supplementary Fig. 22), we conclude that DCBQ does not tightly bind to the chlorophylls at the core of the reaction centre. Instead, DCBQ most likely interacts with peripheral chlorophyll pigments protruding from the protein scaffold of the photosystems, thereby interacting with the highly delocalized charge-transfer state formed after the initial photo-excitation (Fig. 2a, also see Supplementary Information for in-depth discussion).

On the basis of this assessment, we constructed a simple kinetic model (Supplementary Fig. 14) and applied global analysis techniques to time-resolved TA data from cells to extract the relevant lifetimes. We then used this model to determine how efficiently DCBQ diverts electrons away from the native electron transfer chain (Supplementary Information section 1.5.3.). As highlighted in Fig. 2c, our analysis yielded declining electron transfer lifetimes for increased DCBQ concentration. On the basis of our model and these values, we can estimate that

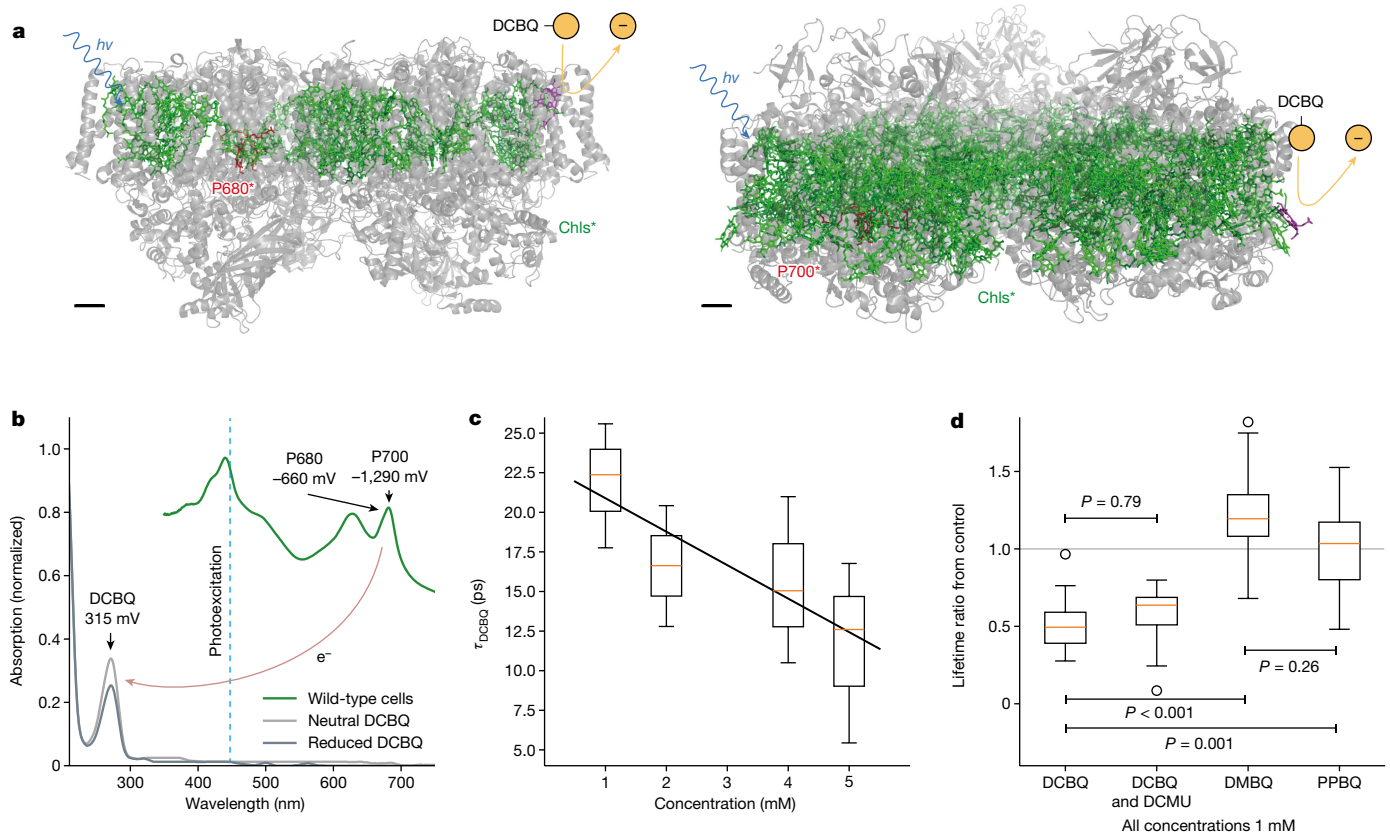

Fig. 2 | Action of quinone electron mediators on wild-type cells. a, Schematic representation of the proposed mechanism of early DCBQ reduction by PSII and PSI. The chlorophylls are photoexcited (Chls*, green), including the special pairs of chlorophylls (P680* and P700*, red in the left most monomer), in a delocalized excited state. The initial charge separated states are formed and rapidly delocalized across the chlorophylls. DCBQ (orange circle) is reduced through a peripheral chlorophyll (purple) that protrudes from the protein scaffold into the thylakoid membrane. PSII crystal structure by Young et al. (Protein Data Bank ID 5TIS)[38]; PSI crystal structure by Jordan et al. (Protein Data Bank ID 1JB0)[4]. Scale bar, 10 Å. **b**, Absorption spectra of *Synechocystis* cells (green), and reduced and neutral DCBQ (greys). **c**, Retrieved electron transfer lifetimes to DCBQ (τ_{DCBQ}). Detail of the model in Supplementary Information section 1.5.2.. The black line is a linear fit to the medians. **d**, Lifetime change on the addition of DCBQ, DMBQ, PPBQ, and DCMU with DCBQ, detail of the model in Supplementary Fig. 14. Presented are the ratios of the additive lifetimes from samples in which no quinone was added (control). A ratio of 1 (grey line) indicates no effect. Student's *t*-test comparisons are overlaid. In **c** and **d**, the box extends from the lower to upper quartile values of the data, the whiskers extend from the box to show the range of the biological replicates ($n = 4$, except DCBQ $n = 5$, and the orange line represents the median).

1 mM DCBQ diverts 17 ± 6% of the initial photoexcited reaction centre population in wild-type *Synechocystis* cells. Critically, this electron transfer occurs as early as 600 fs (Fig. 1d,e), which is consistent with our hypothesis that electrons can be extracted from rapidly formed, delocalized chlorophyll charge-transfer states.

Further support for this mechanistic picture stems from further control experiments with 3-(3,4-dichlorophenyl)-1,1-dimethylurea (DCMU), which binds to the Q_B pocket in PSII (ref. [21]), competing against DCBQ docking and reduction thereafter. Here, the TA measurements with DCBQ and DCMU yielded similar effects to those with only DCBQ, indicating that DCBQ acts at the initial stages of the photosynthetic pathway, rather than only at the Q_B site (Fig. 2d and Supplementary Fig. 15). This trend is also supported by analogous photo-electrochemistry measurements, in which DCBQ was observed to extract electrons at a site that is alternative to the Q_B site (roughly 30% of the photocurrent, Supplementary Fig. 26).

The ability of DCBQ to interact with the photosynthetic electron transport chain at longer timescales was also probed. Photoluminescence decay measurements revealed a reduction in luminescence lifetime with increasing DCBQ concentration, consistent with pulse amplitude modulation fluorometry studies of eukaryotic algal cells in the presence of benzoquinones (Supplementary Fig. 28)[3,14,22]. This is consistent with DCBQ interfering with the photosynthetic electron transport chain beyond the pico-second timescales explored in TA. Oxygen evolution measurements confirmed that PSII continues to perform oxidation of water in vivo in the presence of DCBQ at all concentrations tested in the TA experiments, suggesting the pathway for holes generated by photo-excitation remains active on the addition of DCBQ (Supplementary Fig. 30). However, a long-term cytotoxicity assay revealed that all concentrations of DCBQ greater than 200 µM are cytotoxic to the cells after 12 h, but there was no correlation between the cytotoxicity of benzoquinones and their ability to re-direct electrons from the electron transport chain (Supplementary Fig. 31).

We tested two other common benzoquinone mediators, phenyl-1,4-quinone (PPBQ) and 2,6-dimethyl-1,4-benzoquinone (DMBQ), which have comparable mid-point potentials to DCBQ[14,23]. Figure 2d outlines that the early onset decay in the TA spectrum found for DCBQ was not observed in PPBQ- and DMBQ-treated cells (Supplementary Information section 1.6., Supplementary Fig. 15). Similarly, complementary photo-electrochemistry experiments highlighted that DCBQ was the only benzoquinone screened that was reduced earlier than Q_B in PSII in vivo, as it mediated electron transfer to electrodes in the presence of DCMU (Supplementary Fig. 26). The observation that PPBQ and DMBQ did not demonstrate early interactions with the reaction centres may originate from poor protein–molecule association effects or their lower solubilities in aqueous solutions, which may lead to the quinones being sequestered in intracellular membranes and precipitating in aqueous compartments as they entered the cell[14].

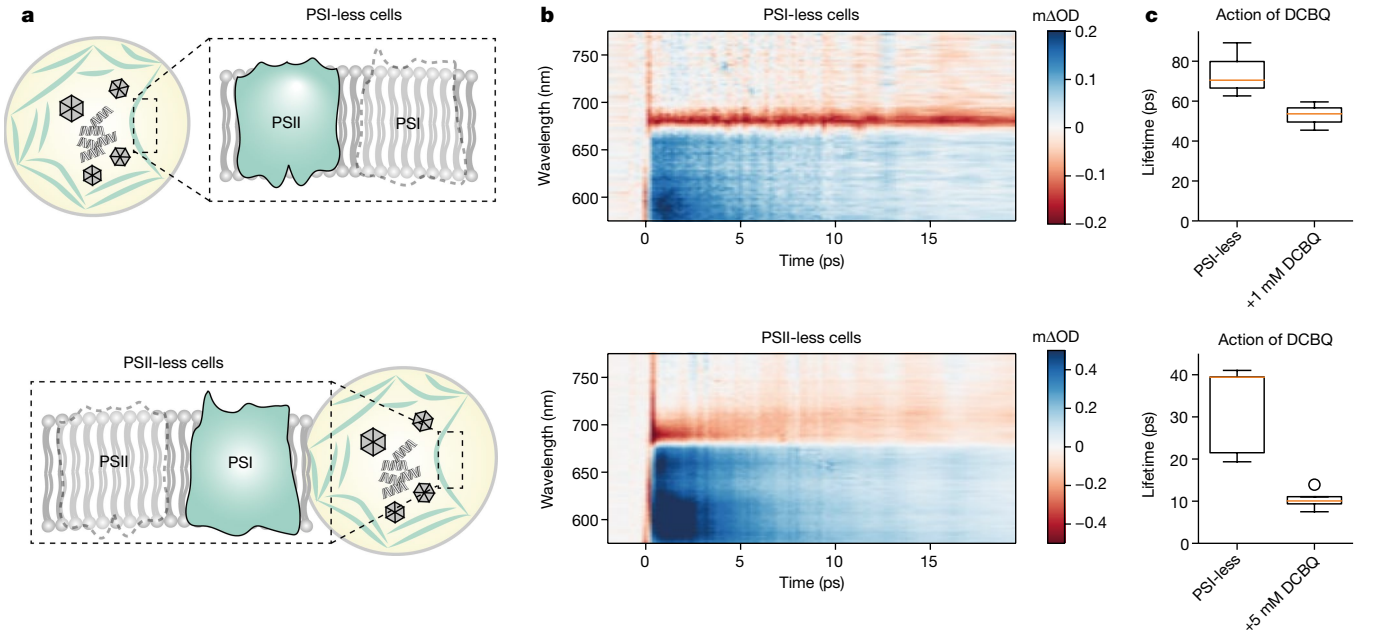

Fig. 3 | Action of DCBQ on cells genetically modified to have only one type of photosystem. a, Schematic representation of photosystem-less mutants analysed (top, PSI-less and bottom, PSII-less). **b**, TA spectra between −2 and 20 ps of cell mutants excited at 450 nm under the same conditions as wild-type cells in their TA spectrum in Fig. 1d (top, PSI-less; bottom, PSII-less). The PSII-less spectrum (bottom) closely resembles that of the wild-type cells. Maps are of one sample, representative of several biological replicates (PSI-less, $n = 4$; PSII-less, $n = 5$). **c**, Lifetimes determined from global analysis in the photosystem-less cells and with the addition of DCBQ (top, PSI-less; bottom, PSII-less). The box extends from the lower to upper quartile values of the data, the whiskers extend from the box to show the range of the biological replicates (PSI-less + DCBQ, $n = 4$; PSII-less + DCBQ, $n = 3$) and the orange line represents the median.

Next, we set out to explain the action of DCBQ electron extraction from different stages of the photosynthetic electron transport chain. To this end, we carried out ultrafast TA spectroscopy on the photosystems in vivo with genetically engineered *Synechocystis* lacking either PSI or PSII intact protein complexes (Fig. 3a). These measurements were further complemented in vitro with isolated photosystems, with and without DCBQ. The full analysis of the data is presented in Supplementary Information. Briefly, the transient response of isolated photosystems shows good agreement with previous reports with PSII dominated by a prominent bleach at 680 nm that decays on the nanosecond timescale[6,24–26], whereas PSI shows a bleach signal at 690 nm and a lower-energy stimulated emission growing in and subsequently decaying on the pico-second timescale between 705 and 720 nm (refs. [27–30]). This latter feature originates from low-energy chlorophylls (so-called 'red forms'), which are present in cyanobacterial PSI cores, albeit their exact spectral position can vary largely in different species[27]. We can therefore confidently assign the transient response to photo-excitation of P680 and P700 in PSII and PSI, respectively.

Whereas the mutant cells and isolated photosystems allow us to deconvolute the spectral features of the reaction centres, the changes in the lifetimes highlight the importance of observing the photodynamics of wild-type cells to obtain accurate insights into the photosynthetic electron transport chain. Following photo-excitation at 450 nm, the PSI-less mutant cells showed spectral features that were markedly different from wild-type cells (Fig. 3b, top panel). The PSI-less cells showed a long-lived bleach at its absorption maximum at 680 nm, lasting longer than a nanosecond. This spectral feature is well matched to that of isolated PSII, but shows a slower decay. This extended ground-state bleach probably arises as the natural charge-extraction pathways were blocked, or not fully functional, due to the absence of functional PSI. By contrast, the PSII-less cells showed more similar dynamics to wild-type cells, with the familiar low-energy spectral feature more than 690 nm also found in isolated PSI (Fig. 3b).

We then studied the effect of DCBQ addition on these mutant cells, as they most closely resemble our in vivo studies (full details in Supplementary Information section 1.7.). On the addition of 1 mM DCBQ to the PSI-less cells, we found a reduction from 74 to 53 ps in the lifetime of the short component of the signal (Fig. 3c, top panel). This suggests that electron extraction by DCBQ treatment from PSII in PSI-less cells occurs over a much longer timescale than the sub-20 ps quenching dynamics observed in the wild-type cells. By contrast, on the addition of 1 mM DCBQ to PSII-less cells, we found a reduction in the lifetimes that closely resembled the behaviour in wild-type cells.

Measurements of living cells are advantageous compared to the those of in vitro systems due to the robustness of the cells and the ability to study altered pathways produced by means of genetic engineering. However, in vitro measurements are useful in identifying spectral features due to their relative simplicity. Measurements of isolated PSI and PSII showed similar spectral features (Supplementary Information section 1.7.) and lifetime reductions compared to mutant cells on the addition of DCBQ, further supporting our assignments and proposed mechanism. Considering the in vitro and in vivo measurements together, we conclude that in the experimental arrangement described here, we primarily resolve electron transfer from PSI to DCBQ. This is in line with the more accessible nature of PSI compared to PSII. Although PSII is also weakly accessible to DCBQ in the PSI-less cells, no corresponding long-lived signal is observed in the wild-type cells that can be directly assigned to PSII with sufficient statistical certainty.

Whereas the fast kinetics of DCBQ reduction by PSI in vivo is desirable, the positive mid-point potentials of benzoquinones limit the power densities they can generate or redox reactions they can catalyse in semi-artificial photosynthesis[31]. To test whether alternative classes of mediators can also extract charge through this non-classical pathway, methyl viologen ($MV^{2+}/MV^{+\cdot} = -0.325$ V versus SHE at pH 7)[32] was investigated. Methyl viologen is the most common synthetic mediator used in reductive catalysis and could unlock greater energy densities compared to DCBQ while bridging the gap between natural and artificial

photosynthesis. Our results are consistent with methyl viologen also being able to extract charge from PSI chlorophylls at the pico-second timescale in isolated PSI (Supplementary Fig. 20). This demonstrates that ultrafast electron extraction from photosystems is not limited to any one class of mediator molecules and opens new opportunities in mediator design and chemical generation.

Conclusion and outlook

Taken together, our results show that in vivo electron transfer from photosynthesis to various exogenous electron mediators is possible directly from the initially photoexcited states of the photosystems, that is, from the earliest possible step in the photosynthetic electron transport chain. This opens new possibilities for re-wiring biological photosynthesis and creates a link between biological and artificial photosynthesis. For example, manipulation of this non-classical pathway could mitigate the losses associated with light stress in biotechnological and agricultural applications, or help to channel charges out for alternative uses in power and chemical generation. Furthermore, these results call for a re-examination of mediated electron transfer strategies, which have long been used to study photosynthesis as well as for enhancing the performance of bioelectrochemical devices such as biophotovoltaics[33]. We also show that the pico-second charge-extraction pathway is not limited to one class of mediators, suggesting that the bioengineering of endogenous mediators, cascades and other biohybrid approaches could be used in the future to expand on and optimize this pathway.

These results also yield new insights into photosynthesis. Contrary to the current understanding that the excited reaction centres are insulated within the photosystem protein scaffold, the action of DCBQ and methyl viologen demonstrate that the scaffold is leaky. This is a potentially significant route in the cell for loss of electrons that might otherwise be used for photosynthesis and may have a role in photoprotection or be a key cause of cell damage from production of reactive oxygen species. More generally, our work highlights that in vivo ultrafast TA spectroscopic measurements are feasible and shows rich information on photoexcited dynamics of living systems. This could be a powerful new tool for understanding photosynthesis bioenergetics and its regulation, especially under conditions of light stress.

Online content

Any methods, additional references, Nature Portfolio reporting summaries, source data, extended data, supplementary information, acknowledgements, peer review information; details of author contributions and competing interests; and statements of data and code availability are available at https://doi.org/10.1038/s41586-023-05763-9.

1. Grattieri, M., Beaver, K., Gaffney, E. M., Dong, F. & Minteer, S. D. Advancing the fundamental understanding and practical applications of photo-bioelectrocatalysis. *Chem. Commun.* **56**, 8553–8568 (2020).
2. Zhang, J. Z. & Reisner, E. Advancing photosystem II photoelectrochemistry for semi-artificial photosynthesis. *Nat. Rev. Chem.* **4**, 6–21 (2020).
3. Fu, H.-Y. et al. Redesigning the QA binding site of Photosystem II allows reduction of exogenous quinones. *Nat. Commun.* **8**, 15274 (2017).
4. Jordan, P. et al. Three-dimensional structure of cyanobacterial photosystem I at 2.5 Å resolution. *Nature* **411**, 909–917 (2001).
5. Shen, G., Boussiba, S. & Vermaas, W. F. J. *Synechocystis* sp PCC 6803 strains lacking photosystem I and phycobilisome function. *Plant Cell* **5**, 1853 (2007).
6. Berera, R., van Grondelle, R. & Kennis, J. T. M. Ultrafast transient absorption spectroscopy: principles and application to photosynthetic systems. *Photosynth. Res.* **101**, 105–118 (2009).
7. Harris, E. H. Chlamydomonas as a model organism. *Annu. Rev. Plant Physiol. Plant Mol. Biol.* **52**, 363–406 (2001).
8. Suda, S. et al. Taxonomic characterization of a marine *Nannochloropsis* species, *N. oceanica* sp. nov. (Eustigmatophyceae). *Phycologia* **41**, 273–279 (2019).
9. Park, S. et al. Chlorophyll–carotenoid excitation energy transfer and charge transfer in *Nannochloropsis oceanica* for the regulation of photosynthesis. *Proc. Natl Acad. Sci. USA* **116**, 3385–3390 (2019).
10. Howe, C. J., Barbrook, A. C., Nisbet, R. E. R., Lockhart, P. J. & Larkum, A. W. D. The origin of plastids. *Philos. Trans. R. Soc. B: Biol. Sci.* **363**, 2675–2685 (2008).
11. Lea-Smith, D. J. et al. Hydrocarbons are essential for optimal cell size, division, and growth of cyanobacteria. *Plant Physiol.* **172**, 1928–1940 (2016).
12. Fălămas, A., Porav, S. A. & Tosa, V. Investigations of the energy transfer in the phycobilisome antenna of *Arthrospira platensis* using femtosecond spectroscopy. *Appl. Sci.* **10**, 4045 (2020).
13. Kopczynski, M. et al. Ultrafast transient lens spectroscopy of various C40 carotenoids: lycopene, β-carotene, (3R,3′ R)-zeaxanthin, (3R,3′ R,6′ R)-lutein, echinenone, canthaxanthin, and astaxanthin. *Phys. Chem. Chem. Phys.* **7**, 2793–2803 (2005).
14. Longatte, G. et al. Investigation of photocurrents resulting from a living unicellular algae suspension with quinones over time. *Chem. Sci.* **9**, 8271–8281 (2018).
15. Evans, M. C. W. & Heathcote, P. Effects of glycerol on the redox properties of the electron acceptor complex in spinach Photosystem I particles. *Biochim. Biophys. Acta Bioenerg.* **590**, 89–96 (1980).
16. De Causmaecker, S., Douglass, J. S., Fantuzzi, A., Nitschke, W. & Rutherford, A. W. Energetics of the exchangeable quinone, Q_B, in Photosystem II. *Proc. Natl Acad. Sci. USA* **116**, 19458–19463 (2019).
17. Stirbet, A. Excitonic connectivity between photosysstem II units: what is it, and how to measure it? *Photosynth. Res.* **116**, 189–214 (2013).
18. Mirkovic, T. et al. Light absorption and energy transfer in the antenna complexes of photosynthetic organisms. *Chem. Rev.* **117**, 249–293 (2017).
19. Ma, F., Romero, E., Jones, M. R., Novoderezhkin, V. I. & van Grondelle, R. Both electronic and vibrational coherences are involved in primary electron transfer in bacterial reaction center. *Nat. Commun.* **10**, 933 (2019).
20. Dods, R. et al. Ultrafast structural changes within a photosynthetic reaction centre. *Nature* **589**, 310–314 (2021).
21. Trebst, A. The three-dimensional structure of the herbicide binding niche on the reaction center polypeptides of photosystem II. *Z. Naturforsch. C J. Biosci.* **42**, 742–750 (1987).
22. Longatte, G. et al. Evaluation of photosynthetic electrons derivation by exogenous redox mediators. *Biophys. Chem.* **205**, 1–8 (2015).
23. O'Reilly, J. E. Oxidation-reduction potential of the ferro-ferricyanide system in buffer solutions. *Biochim. Biophys. Acta Bioenerg.* **292**, 509–515 (1973).
24. Durrant, J. R. et al. Subpicosecond equilibration of excitation energy in isolated photosystem II reaction centers. *Proc. Natl Acad. Sci. USA* **89**, 11632–11636 (1992).
25. Groot, M. L. et al. Initial electron donor and acceptor in isolated Photosystem II reaction centers identified with femtosecond mid-IR spectroscopy. *Proc. Natl Acad. Sci. USA* **102**, 13087–13092 (2005).
26. Klug, D. R., Durrant, J. R. & Barber, J. The entanglement of excitation energy transfer and electron transfer in the reaction centre of photosystem II. *Philos. Trans. R. Soc. London, Ser. A* **356**, 449–464 (1998).
27. Russo, M., Casazza, A. P., Cerullo, G., Santabarbara, S. & Maiuri, M. Ultrafast excited state dynamics in the monomeric and trimeric photosystem I core complex of *Spirulina platensis* probed by two-dimensional electronic spectroscopy. *J. Chem. Phys.* **156**, 164202 (2022).
28. Slavov, C., Ballottari, M., Morosinotto, T., Bassi, R. & Holzwarth, A. R. Trap-limited charge separation kinetics in higher plant photosystem I complexes. *Biophys. J.* **94**, 3601–3612 (2008).
29. Lee, Y., Gorka, M., Golbeck, J. H. & Anna, J. M. Ultrafast energy transfer involving the red chlorophylls of cyanobacterial photosystem I probed through two-dimensional electronic spectroscopy. *J. Am. Chem. Soc.* **140**, 11631–11638 (2018).
30. Shelaev, I. V. et al. Femtosecond primary charge separation in *Synechocystis* sp. PCC 6803 photosystem I. *Biochim. Biophys. Acta Bioenerg.* **1797**, 1410–1420 (2010).
31. Weliwatte, N. S., Grattieri, M. & Minteer, S. D. Rational design of artificial redox-mediating systems toward upgrading photobioelectrocatalysis. *Photochem. Photobiol. Sci.* **20**, 1333–1356 (2021).
32. Bennett, T. et al. Elucidating the role of methyl viologen as a scavenger of photoactivated electrons from photosystem I under aerobic and anaerobic conditions. *Phys. Chem. Chem. Phys.* **18**, 8512–8521 (2016).
33. Wey, L. T. et al. The development of biophotovoltaic systems for power generation and biological analysis. *Chem. Electro. Chem.* **6**, 5375–5386 (2019).
34. Kato, M., Zhang, J. Z., Paul, N. & Reisner, E. Protein film photoelectrochemistry of the water oxidation enzyme photosystem II. *Chem. Soc. Rev.* **43**, 6485–6497 (2014).
35. Lea-Smith, D. J., Bombelli, P., Vasudevan, R. & Howe, C. J. Photosynthetic, respiratory and extracellular electron transport pathways in cyanobacteria. *Biochim. Biophys. Acta, Bioenerg.* **1857**, 247–255 (2016).
36. Kurashov, V. et al. Critical evaluation of electron transfer kinetics in P700–FA/FB, P700–FX, and P700–A1 Photosystem I core complexes in liquid and in trehalose glass. *Biochim. Biophys. Acta Bioenerg.* **1859**, 1288–1301 (2018).
37. Setif, P. Q. Y. & Bottin, H. Laser flash absorption spectroscopy study of ferredoxin reduction by photosystem I: spectral and kinetic evidence for the existence of several photosystem I-ferredoxin complexes. *Biochemistry* **34**, 9059–9070 (1995).
38. Young, I. D. et al. Structure of photosystem II and substrate binding at room temperature. *Nature* **540**, 453–457 (2016).

Methods

Biological samples

Cell culture and growth conditions. *Synechocystis* sp. PCC 6803 (*Synechocystis*) cells were cultured photoautotrophically under 50 $\mu mol_{photons}\ m^{-2}\ s^{-1}$ of continuous white light at 30 °C in BG11 medium supplemented with 10 mM $NaHCO_3$ (ref. [39]). Liquid cultures were bubbled with air and shaken at 120 rpm, and 1.5% (w/v) agar was used in solid medium. Culture growth was measured by attenuance at 750 nm (optical density, OD_{750}). Culture chlorophyll concentration (nmol Chl *a* ml^{-1}) was calculated from absorbances at 680 and 750 nm: ($A_{680}-A_{750}$) × 10.814 (ref. [40]). All measurements were taken using a UV-1800 Spectrophotometer (Shimadzu).

Photosystem-less mutants. The modifications to the culturing protocol for the *Synechocystis* photosystem-less mutants are as follows. Wild-type cells were cultured in BG11 with no additives at 30 °C with 40 $\mu mol_{photons}\ m^{-2}\ s^{-1}$ light. PSI-less (*psaAB*$^-$), with 10 μg ml^{-1} chloramphenicol, were cultured in BG11 plus 5 mM glucose, at 30 °C and 5 $\mu mol_{photons}\ m^{-2}\ s^{-1}$ light[5]. PSII-less cells (*psbDIC*$^-$/*psbDII*$^-$) with 10 μg ml^{-1} chloramphenicol and 10 μg ml^{-1} spectinomycin, were cultured in BG11 plus 5 mM glucose at 30 °C with 40 $\mu mol_{photons}\ m^{-2}\ s^{-1}$ light[41].

Olive mutant. The *Synechocystis* Olive mutant was generated previously by markerless disruption of the *cpcBAC1C2* genes[41]. As reported previously, the Olive mutant has no phycocyanin discs in the PBS. The Olive mutant still has the allophycocyanin core of the PBS. Deletion of the entire PBS results in extremely poor growth[41], so this mutant was not analysed in this study.

Isolated photosystems. In this study, whole cells of cyanobacterium *Synechocystis* were compared against PSII and PSI protein complexes isolated from the cyanobacterium *Thermosynechococcus elongatus*. PSII isolated from mesophilic *Synechocystis* is significantly more unstable than those extracted from *T. elongatus*. Previous studies have compared the photo-electrochemistry of PSII in vitro versus in vivo from *T. elongatus* and *Synechocystis*, respectively, for similar stability reasons[42]. The purified *T. elongatus* PSII was provided by the group of A.W. Rutherford (Imperial College London, UK). PSII dimers were isolated from *T. elongatus* using methods previously reported[43]. The PSII stock had a chlorophyll concentration of 2.4 mg ml^{-1} in 2-(*N*-morpholino)ethanesulfonic acid (MES) storage buffer (10% glycerol, 15 mM $MgCl_2$, 15 mM $CaCl_2$, 1 M betaine, 40 mM MES (pH 6.5)). Purified PSI trimers were isolated from *T. elongatus* using methods previously reported[44]. The PSI stock had a chlorophyll concentration of 9.07 mg ml^{-1} in MES storage buffer. Isolated photosystems were stored in small aliquots in a liquid N_2 Dewar flask, and a new aliquot was thawed on each day of experiments. Photo-electrochemistry and spectroscopy measurements on isolated photosystems were conducted in MES buffer (50 mM KCl, 15 mM $CaCl_2$, 15 mM $MgCl_2$, 40 mM MES (pH 6.5)). The *T. elongatus* was cultured at 60 °C, the spectroscopy suite was maintained at less than 21 °C and the photo-electrochemistry set-up was controlled at 25 °C. Preparation methods for spectroscopy has been reported previously[45].

Chemicals

Unless otherwise stated, all materials used throughout this research were purchased from commercial suppliers and used without further purification. The exogenous electron mediators used in this study were (Supplementary Fig. 32): DCBQ (98%, Sigma-Aldrich), PPBQ (95%, ACROS Organics), DMBQ (97% Sigma-Aldrich) and MV^{2+} (Sigma-Aldrich). Benzoquinone candidates were selected from previous studies with *Chlamydomonas reinhardtii* by the group of F. Lemaître[3,14,22,46]. The photosynthetic electron transport chain inhibitor used in this study was DCMU (98%, Alfa Aesar). DCMU was used as an inhibitor of PSII at the Q_B site[21]. Stocks of 100 mM DCBQ, 100 mM MV^{2+} and 100 mM DCMU were made in dimethylsulfoxide (DMSO) for addition to biological samples. Stocks of 10 mM DMBQ and PPBQ were made in ethanol for addition to biological samples, with 8.2 mM SDS where specified.

Ultrafast TA spectroscopy

Pico-second TA measurements were performed as previously reported[47,48]. In brief, we used an Yb-based amplified system (PHAROS, Light Conversion) providing 14.5 W at 1,030 nm and a 38 kHz repetition rate. The probe beam is generated by focusing a portion of the fundamental in a 4 mm YAG substrate to generate a white light that spans 520 to 900 nm. The pump beam is generated by seeding a portion of the fundamental to a narrow band optical parametric oscillator (ORPHEUS-LYRA, Light Conversion). The pump pulse was set to 450 nm, unless otherwise indicated. The sample solutions were placed in 1 mm path length cuvettes (Hellma). The pump and probe beams were focused to sizes of 280 × 240 and 55 × 67 μm, respectively. The probe is delayed relative to the pump using a computer-controlled translation stage (Newport), and a chopper wheel (Thorlabs) modulated the pump beam to gain access to differential TA spectra. The probe pulses transmitted through the sample were detected on a single-shot basis by a line camera (Stemmer Imaging). All measurements presented in our work were acquired within 15 min of loading the sample. Further control experiments exposed the cells to the laser for 120 min (eightfold longer).

Time-correlated single-photon counting

To record the time-resolved photoluminescence decay of the samples, time-correlated single-photon counting (TCSPC) was performed. Samples were excited with a pulsed laser (PicoQuant LDH-400-B and LDH-470-B (at up to 40 MHz, typically operated at 2.5 MHz)) at either 407 or 470 nm, with the resulting photoluminescence decay collected on at 680 ± 10 nm. Diode lasers were controlled by a trigger box/power supply unit (PDL 800-B, PicoQuant). TCSPC used an emission spectrometer (Lifespec-ps unit, VTC900 PCI card, Edinburgh Instruments) with a multi-channel plate detector (R3809U-50, Hamamatsu). The instrument response was determined by scattering excitation light into the detector using a piece of frosted glass; a value of 265 ps was obtained. Pulse energy was 2 pJ. Pulse width of the diode lasers were measured to be 80 ps (full-width at half-maximum).

Spectroelectrochemistry

Solutions of DCBQ (1 mM) in BG11 medium and MES buffer were prepared. The DCBQ solution (1 ml) was loaded into an optically transparent thin-layer electrochemical cuvette with a pseudo reference electrode (Ag wire). Cyclic voltammetry was performed (applied potential 0.5 to −0.2 V versus pseudo reference Ag wire, scan rate: 0.05 V s^{-1}) to determine that the working electrode poised at −0.1 V would reduce the DCBQ. The ultraviolet-visible light spectrometer was baselined with a solution of 1% DMSO (v/v) in BG11 medium or MES buffer as appropriate. The spectrum of the DCBQ solution was measured without applying a potential (neutral form). Chronoamperometry experiments were performed at −0.1 V. At 30 min into the chronoamperometry, the spectrum of the DCBQ (doubly reduced form) solution was measured.

Photo-electrochemistry

All photoelectrochemical measurements were performed at 25 °C under atmospheric conditions using an Ivium Technologies CompactStat, with an Ag/AgCl (saturated KCl) reference electrode (corrected by +0.197 V for SHE) and a platinum mesh counter electrode. Chronoamperometry experiments were performed at an applied potential 0.5 V versus SHE. Chronoamperometry experiments were performed at a sampling rate of 1 s^{-1}, under light and dark cycles using a collimated

LED light source (50 $\mu mol_{photons}\ m^{-2}\ s^{-1}$, roughly 1 mW cm^{-2} equivalent, 680 nm, Thorlabs).

Protein-film photo-electrochemistry. Inverse opal indium-tin oxide (IO-ITO) electrodes with 750 nm pore sizes were prepared using a previously reported method[43]. Protein-film photo-electrochemistry was performed as previously reported[42]. In brief, a one-in-three dilution of the 2.4 mg ml^{-1} (77 μM) stock solution of isolated PSII was made immediately before adsorption on the electrodes to give a final concentration of 25.6 μM. A small aliquot (1 μl) of the new solution was drop-cast onto 750 nm IO-ITO electrodes and left to stand for 15 min in a closed Petri dish in the dark before being used in photoelectrochemical experiments. The electrolyte was MES buffer (pH 6.5). Light/dark cycles (15 s on/15 s off) were used.

Cell photo-electrochemistry. IO-ITO electrodes with 10 μm macropores and 3 μm interconnecting channels at a thickness of 40 μm were prepared using the method previously reported[42]. Photo-electrochemistry of cyanobacterial cells was performed as previously reported[49]. In brief, planktonic cultures of early stationary phase cyanobacterial cells at an attenuance at OD_{750} of around 1 were concentrated by centrifugation at 5,000*g* for 10 min, the supernatant removed, and the pellet resuspended in fresh BG11 medium to a concentration of 150 nmol Chl *a* ml^{-1}. This solution (250 μl) was drop-cast onto the IO-ITO electrodes and left overnight at room temperature in a humid chamber in the dark to allow cell penetration and adhesion, yielding cell-loaded electrodes that were used for analysis 16 h later. The electrolyte was BG11 medium (pH 8.5). Light/dark cycles (60 s on/90 s off) were used.

Oxygen evolution measurements

Oxygen evolution measurements were made using a Clark electrode consisting of an Oxygraph Plus Electrode Control Unit, S1 Oxygen Electrode Disc, DW2/2 Electrode Chamber and a LED1 High Intensity LED Light Source (Hansatech Instruments). Measurements were performed on 1.5 ml samples of wild-type *Synechocystis* cells containing 10 μg ml^{-1} of Chl *a* in BG11 supplemented with different concentrations of DCBQ. Measurements were collected at 25 °C with 1 min of darkness, followed by 1 min of 1,500 $\mu mol_{photons}\ m^{-2}\ s^{-1}$ light at 627 nm (equivalent to 28.65 mW cm^{-2}). The rate of oxygen production in the dark was subtracted from that in the light and normalized to Chl *a* content. Data were collected from five biological replicates, each with three technical replicates.

Cytotoxicity assays

Wild-type *Synechocystis* cells (5 nmol Chl *a*) were incubated with different concentrations of exogenous mediator for 24 h. *Synechocystis* cells incubated in BG11 with no electron mediator or in BG11 with 5% (v/v) DMSO solvent under the same conditions were used as controls. Following incubation, the cells were resuspended in fresh BG11 and their concentration was standardized to an OD_{750} of 0.5. Aliquots (10 μl) of three serial dilutions (×1, $\times 10^{-3}$, $\times 10^{-6}$) were spotted on BG11 agar plates, which were then incubated for 1 week at 30 °C and 50 $\mu mol_{photons}\ m^{-2}\ s^{-1}$ light. The growth of the cells pre-incubated with mediator was compared to the controls to assess the cytotoxicity of the mediators.

Statistics

The ratios of the lifetime of samples on the addition of benzoquinones and DCMU compared to when nothing was added were compared using Student's *t*-tests.

Data availability

The data underlying all figures in the main text are publicly available from the University of Cambridge repository at https://doi.org/10.17863/CAM.92167.

Code availability

All code used in this work is available from the corresponding authors upon reasonable request.

39. Stanier, R. Y., Kunisawa, R., Mandel, M. & Cohen-Bazire, G. Purification and properties of unicellular blue-green algae (order Chroococcales). *Bacteriol. Rev.* **35**, 171–205 (1971).
40. Lea-Smith, D. J. et al. Thylakoid terminal oxidases are essential for the cyanobacterium *Synechocystis* sp. PCC 6803 to survive rapidly changing light intensities. *Plant Physiol.* **162**, 484–495 (2013).
41. Lea-Smith, D. J. et al. Phycobilisome-deficient strains of *Synechocystis* sp PCC 6803 have reduced size and require carbon-limiting conditions to exhibit enhanced productivity. *Plant Physiol.* **165**, 705–714 (2014).
42. Zhang, J. Z. et al. Photoelectrochemistry of photosystem II in vitro vs in vivo. *J. Am. Chem. Soc.* **140**, 6–9 (2018).
43. Mersch, D. et al. Wiring of photosystem II to hydrogenase for photoelectrochemical water splitting. *J. Am. Chem. Soc.* **137**, 8541–8549 (2015).
44. El-Mohsnawy, E. et al. Structure and function of intact photosystem 1 monomers from the cyanobacterium *Thermosynechococcus elongatus*. *Biochemistry* **49**, 4740–4751 (2010).
45. Paul, N. *Intermolecular Photophysics of Photosystem II Core Complexes at Protein-Nanomaterial Interfaces*. PhD thesis, Univ. Cambridge (2015).
46. Longatte, G., Rappaport, F., Wollman, F.-A., Guille-Collignon, M. & Lemaître, F. Mechanism and analyses for extracting photosynthetic electrons using exogenous quinones–what makes a good extraction pathway? *Photochem. Photobiol. Sci.* **15**, 969–979 (2016).
47. Pandya, R., MacQueen, R. W., Rao, A. & Davies, N. J. L. K. Simple and robust panchromatic light harvesting antennacomposites via FRET engineering in solid state host matrices. *J. Phys. Chem. C.* **122**, 22330–22338 (2018).
48. Hinrichsen, T. F. et al. Long-lived and disorder-free charge transfer states enable endothermic charge separation in efficient non-fullerene organic solar cells. *Nat Commun.* **11**, 5617 (2020).
49. Wey, L. T. et al. A biophotoelectrochemical approach to unravelling the role of cyanobacterial cell structures in exoelectrogenesis. *Electrochim. Acta* **395**, 139214 (2021).

Acknowledgements We acknowledge W. Vermaas (Arizona State University, USA) for the gift of the photosystem-less mutants used in this study and W. Rutherford (Imperial College London) for the gift of isolated PSII as well as valuable discussions on this project. We thank X. Chen for provision of porous electrodes. We acknowledge F. Lemaitre (École Normale Supérieure, France) and P. Rich (University College of London, UK) for helpful discussions about exogenous benzoquinones and photosynthetic microorganisms. We thank K. Redding for helpful discussions on photoexcited states of reaction centre proteins. C.S. and T.K.B. thank V. Gray for insightful discussion at the start of the project. We acknowledge N. Paul for his PhD work, which contributed ideas to this study. T.K.B. gives thanks to the Centre for Doctoral Training in New and Sustainable Photovoltaics (grant no. EP/L01551X/2) and the NanoDTC (grant no. EP/L015978/1) for financial support. L.T.W. acknowledges financial support from the Cambridge Trust. C.S. acknowledges financial support by the Royal Commission of the Exhibition of 1851. We acknowledge financial support by the BBSRC (grant no. BB/R011923/1 to J.Z.Z.), the EPSRC (grant no. EP/M006360/1) and the Winton Program for the Physics of Sustainability as well as from the Deutsche Forschungsgemeinschaft within the framework of the Research Training Group 2341 'MiCon'. This project has received funding from the European Research Council under the European Union's Horizon 2020 research and innovation programme (grant agreement nos. 758826, 764920 and 682833).

Author contributions T.K.B. and L.T.W. contributed equally to the work and initially developed the application of ultrafast techniques to exame cyanobacteria. C.S. and A.R. supervised the spectroscopy, C.J.H. supervised the cell work, J.Z.Z. developed the research question. T.K.B. performed the TA and TCSPC experiments and the analysis, and prepared the figures. L.T.W. chose and prepared the samples for TA and TCSPC, performed the photo-electrochemistry, oxygen evolution, cytotoxicity and microscopy experiments, and did protein crystal structure analysis. J.M.L. prepared samples for the MV^{2+} study. H.M. prepared isolated PSI. T.K.B., L.T.W., M.M.N., R.H.F., E.R., C.S., J.Z.Z., C.J.H. and A.R. contributed to discussions, analysis and writing of the manuscript.

Competing interests The authors declare no competing interests.

Additional information

Supplementary information The online version contains supplementary material available at https://doi.org/10.1038/s41586-023-05763-9.

Correspondence and requests for materials should be addressed to Christopher J. Howe, Christoph Schnedermann, Akshay Rao or Jenny Z. Zhang.

Peer review information *Nature* thanks the anonymous reviewers for their contribution to the peer review of this work. Peer reviewer reports are available.